Available online at www.sciencedirect.com
SCIENCE DIRECT®
Thin Solid Films 440 (2003) 54–59
thin solid films
www.elsevier.com/locate/tsf

# Magnetic properties of sputtered soft magnetic Fe–Ni films with an uniaxial anisotropy

Jung Gi Kim[a], Kyung Hunn Han[a,*], Seok Ho Song[a], Anne Reilly[b]

[a]*Department of Physics, Hanyang University, Seoul 133-791, South Korea*
[b]*Department of Physics, College of William and Mary, Williamsburg, VA 23187-8795, USA*

Received 6 January 2003; received in revised form 28 April 2003; accepted 16 May 2003

**Abstract**

The microstructure and magnetic properties of polycrystalline $Fe_{100-x}Ni_x$ films have been studied by X-ray diffraction (XRD) and magnetic moment measurements. In the XRD pattern of Fe–Ni films, the values of area ratio, $A(1\,1\,1)/A(2\,0\,0)$ for the XRD peaks, in the thickness dependence decrease rapidly with increasing film thickness in the films with a bias field applied parallel to the plane in order to introduce uniaxial anisotropy, but the values for the films without the field are nearly constant. The coercivity vs. thickness analyzed by using Néel's formula show that the values for the films with the bias field follow Néel's formula within the thickness range of 40–100 nm, except the range of 10–40 nm. This result indicates that there is a change in domain wall type at the thickness of 40 nm. From the results of thickness and temperature dependence of magnetization analyzed by using some theoretical models, the values of interaction strength between magnetic ions were determined. The electrical resistivity of films is found to be consistent with the Mayadas–Shatzkes model.


*Keywords:* X-ray diffraction; Fe–Ni film; Magnetic hysteresis; Spin-wave; Uniaxial anisotropy

## 1. Introduction

The most prominent feature of the $Fe_{100-x}Ni_x$ ($35 < x < 40$) alloy system is a nearly vanishing thermal expansion coefficient, that is also known as the Invar effect discovered by Guillaume in 1897 [1]. The property of magnetic moment of the Fe–Ni alloys shows an anomalous behavior with substantial deviations from the Slater–Pauling curve [2]. Over the past few decades, a considerable number of studies have been conducted on the thermal phenomenon [3] and band-structure [4] of Fe–Ni alloy. Little attention has been given to magnetic properties of the Invar alloy.

The uniaxial anisotropy is usually called magnetization-induced, rather than field-induced anisotropy [5]. The uniaxial anisotropy can be controlled in several ways. The method most frequency applied is annealing in a magnetic field. The uniaxial anisotropy can also be induced by applying a magnetic field during deposition. Magnetic uniaxial anisotropy in the films plays the most important role in the technical magnetization. The magnetization behavior is a function of thickness and temperature, which has been predicted by various mean-field [6], spin-wave density [7], and spin-fluctuation theories [8]. In addition, the dependence on thickness may predict the property of the mono-atomic layer by extrapolating to 0 Å. The coercivity is determined not only by the microstructure (grain size, porosity, stress) created by the deposition conditions but also the change in the domain wall type. In this paper we report the magnetic properties of Fe–Ni films with thickness below 100 nm deposited with additional constant magnetic bias field.

## 2. Experiment

DC magnetron sputtering system was used in sample fabrication, together with a hybrid target consisting of Ni chips placed on Fe disc with purity better than 99.9% covering 9.9% of the disc surface. Films of 8 mm in

*Corresponding author. Tel.: +82-2-2290-0919; fax: +82-2-2295-6868.
*E-mail address:* ilywamh@ihanyang.ac.kr (K.H. Han).

0040-6090/03/$ - see front matter © 2003 Elsevier B.V. All rights reserved.
doi:10.1016/S0040-6090(03)00829-0

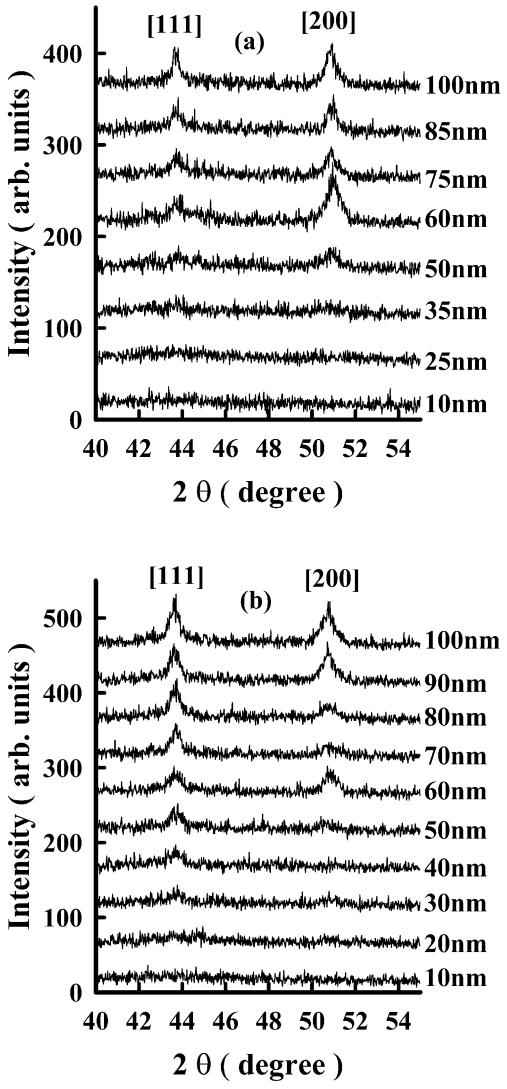


Fig. 1. XRD patterns at a shown thickness for the film F1(a) and F2(b).

diameter were deposited on square Pyrex 7740 glass substrates of area 10×10 mm. The sputtering chamber was first evacuated to $3\times10^{-7}$ Torr or better and then sputtering was conducted in an Ar gas pressure of 1 mTorr. The sputtering power and substrate temperature were held at 50 W and approximately 450 °C throughout the experiments, respectively. During deposition an additional constant magnetic bias field of 500 G was applied to the film parallel to the plane in order to introduce uniaxial anisotropy. The films without the magnetic bias field $H_{\text{bias}}$ are called F1 and the films with magnetic bias are called F2. The crystal structure and composition were investigated by using X-ray diffraction (XRD) with Cu Kα radiation in θ–2θ geometry and Energy Dispersive X-ray Spectrometer (EDS). Magnetic measurements were performed by vibrating sample magnetometry (VSM) with a magnetic field of 100 G at room temperature, and the electrical resistivity was measured by using the d.c. four-point probe method.

## 3. Results and discussion

### 3.1. X-ray diffraction

The crystal structure of the films was confirmed by X-ray diffractometer (XRD). Fig. 1 gives the XRD patterns for the film F1(a) and F2(b) at shown film thickness. As shown in Fig. 1, the reflection peak of (1 1 1) at different films thickness for the film F2 shows stronger preferred orientation than that of (2 0 0) as decreasing the film thickness except the film of 60 nm. The results of XRD show that the films have a crystal structure of face-centered cubic (fcc) without any other crystal phase. The Ni concentration in the $Fe_{100-x}Ni_x$ films is determined to be $x=41$ using EDS measurement, which is in good agreement with the value of JCPDS card [9].

For cubic metals such as iron and nickel the magnetic moments align preferentially along ⟨1 0 0⟩ and ⟨1 1 1⟩ axis, respectively. In fcc Ni, the magnetization has an easy-axis in the ⟨1 1 1⟩ directions, a medium-axis in the ⟨1 1 0⟩, and a hard-axis in the ⟨1 0 0⟩ [10]. Fig. 2a shows the thickness dependence of the XRD peak area ratio, $A(1\,1\,1)/A(2\,0\,0)$, for the film F1 and F2. As shown in Fig. 2a the area ratio for the film F1 is nearly constant, but the values for the film F2 decrease with increasing film thickness. The lattice constants as shown in Fig. 2b increase at the rate of $(1.1\pm0.1)\times10^{-5}$ with increasing films thickness and can be compared with 3.595 Å of $Fe_{64}Ni_{36}$ [11].

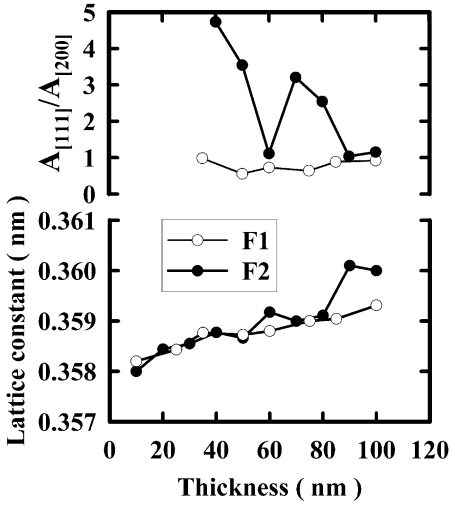


Fig. 2. Area ratio (a) and lattice constant (b) of Fe–Ni films as a function of film thickness.

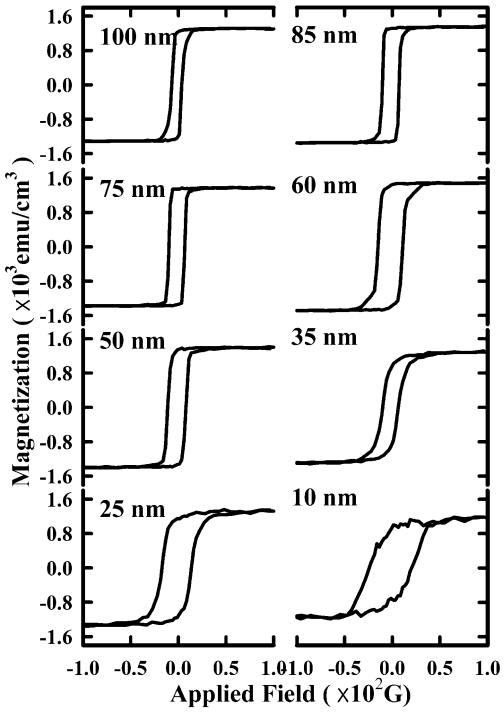


Fig. 3. Magnetic hysteresis loops for an external field applied parallel to the in-plane direction of film F1.

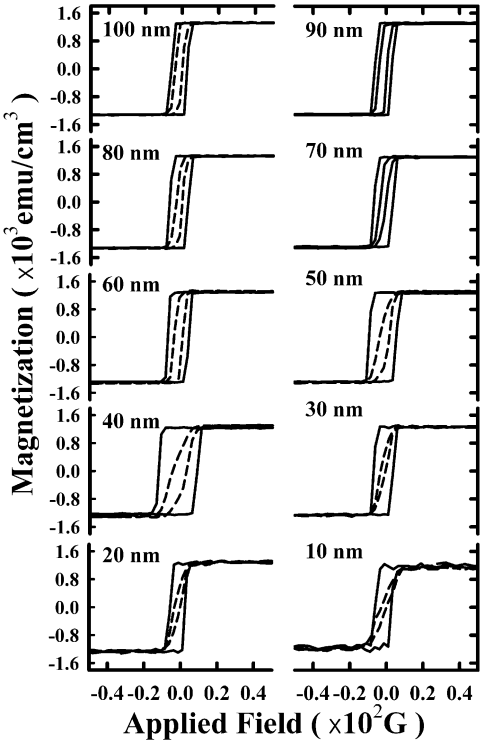


Fig. 4. Hysteresis loops of film F2 for the external magnetic field along $H_{bias} \| H$ (Solid line) and $H_{bias} \perp H$ (Dash line) on the in-plane of film, where $H_{bias} \| H$ and $H_{bias} \perp H$ mean the direction of applied magnetic filed $H$ with respect to $H_{bias}$.

### 3.2. Magnetic hysteresis loops

The magnetic hysteresis loops for Fe–Ni films are shown in Fig. 3 (F1) and Fig. 4 (F2). We evaluated here an anisotropy field $H_k$ for the film F2 using Stoner–Wolhfarth (S–W) model [12] under the assumption that the magnetization process of Fe–Ni proceeds via a coherent rotation of magnetization at the magnetic field of above 100 G. In the S–W model the susceptibility $\chi$ at $H=0$ ($\chi_{H=0}=\left.\frac{dM}{dH}\right|_{H=0}$) for polycrystalline films is given by $\chi_{H=0}=M_s\sin^2\theta_0/H_k$ [12], where $\theta_0$ is the angle between induced anisotropic uniaxial axis and external applied field and $M_s$ the saturation magnetization. The anisotropic field $H_k$ is, therefore, expressed as $H_k=\sin^2\theta_0 M_s/\chi_{H=0}$ when the angular distribution of domain magnetization is isotropic, $\sin^2\theta_0=2/3$ and can be evaluated by using experimental values of $M_s$ and $\chi_{H=0}$ obtained by a slope of $H_c$. The uniaxial anisotropy constant, $K_u=M_sH_k/2$, was also calculated from $H_k$.

Fig. 5 shows the thickness dependence of $H_k$ and $K_u$ for the film F2. As shown in the figure, the values of $H_k$ and $K_u$ decrease with increasing film thickness except for the film with thickness of 40 nm, which has an anomalously large value. The value of $K_u$ changes from $1.3\times10^3$ erg/cm$^3$ for 100 nm film to $3.5\times10^3$ erg/cm$^3$ for 10 nm film. These values are the same order as the reported values for Fe–Ni bulk material [13].

Fig. 6 shows the thickness dependence of the squareness ratio. As shown in the figure, these values for the films of $H_{bias} \perp H$ (curve 3), where $H$ is an applied magnetic field in VSM measurements, decrease from 50 to 20% with decreasing thickness of films within the thickness range from 10 to 50 nm. The film F2 (curve 1) and F1 (curve 2) have squareness above 90% within the thickness range from 50 to 100 nm. The squareness for most of the films increases with increasing film thickness.

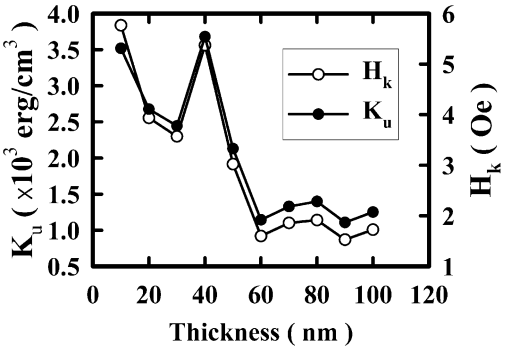


Fig. 5. Thickness dependence of $H_k$ and $K_u$ for the film F2.

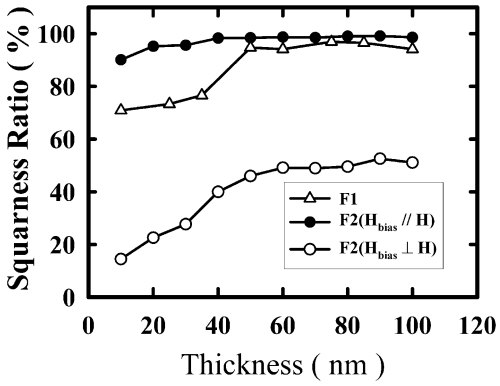


Fig. 6. Squareness ratio as a function of film thickness.

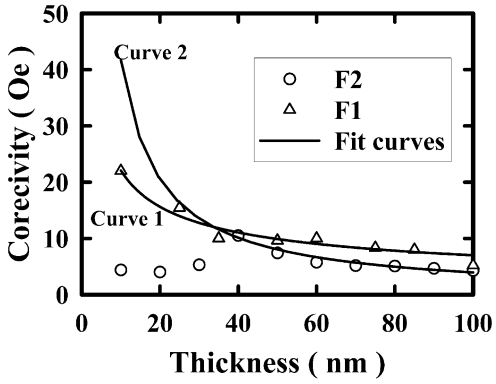


Fig. 7. Coercivity of Fe–Ni films as a function of film thickness for film F1 (curve 1) and F2 (curve 2). The solid curves represent the theoretical values.

### 3.3. Thickness dependence of coercivity

Fig. 7 shows the thickness dependence of the coercivity for film F1 and F2. As shown in Fig. 7, the coercivity decreases within the thickness range of 10–100 nm with increasing the thickness in film F1. But in the case of film F2, the coercivity increases from the thickness of 10 nm up to 40 nm and then begins to decrease with increasing film thickness. Néel derived the well known '4/3' law for the dependence of coercivity on the film thickness $t$, $H_c \propto t^{-4/3}$, which is valid under the assumption that the thickness fluctuation $dt/dx$, where $dt/dx$ is the variation in the film thickness with position, (with $x$ being the lateral direction along which the wall motion occurs) is constant [14]. Calculation of the thickness dependence of the coercivity is performed by general expression as

$$H_c = ct^{-n} \tag{1}$$

where $t$ is a film thickness and $c$, $n$ are fitting constant. The fitting result shows $n = 0.5 \pm 0.1$ (curve 1 of Fig. 7) for the film F1. The value can be compared with $n = 0.4 \pm 0.1$ for ultrathin Co films deposited on Cu-buffered Si(1 1 1) substrate [15]. While the value of $n$ for the film F2 is $1.0 \pm 0.1$ (curve 2 of Fig. 7) within the thickness range of 40–100 nm. As shown in Fig. 7, the Néel formula fits very well to data for the film F1 and F2 over a wide thickness range and within the thickness range 40–100 nm, respectively. Therefore, the dominant coercivity mechanism for this region could be assumed to be the wall motion as predicted by Néel. But the coercivity vs. thickness for film F2 shows a deviation from Néel formula within the thickness range of 10–40 nm. The disagreement with the Néel formula is attributed to the existence of Néel wall rather than a Bloch wall in this thickness range because Néel wall might be expected to occur in the thickness range according to the wall energy theory [16]. It was found that $n$ is dependent on deposition conditions such as applying a magnetic bias field. Also, a transition of wall type is observed at the thickness of 40 nm for the film F2.

### 3.4. Thickness dependence of magnetization

Fig. 8a shows the reduced magnetization of the samples of F1 and F2 as a function of thickness. Their data show that the magnetization for all the samples increases with increasing film thickness. On the other hand, the magnetizations of film F2 are slightly greater than that of film F1 for a given thickness. The thickness dependence of magnetization has been calculated by using various approximation methods [6–8]. According to spin-wave methods [17], the thickness dependence of the magnetization at temperature $T$ for a fcc film is given by the equation

$$\frac{M_S(t)}{M_0} = 1 - \frac{1}{16\pi S^2 G_3}\left(\frac{kT}{J}\right)\sum_{\lambda_3=0}^{G_3}(1+\cos k_3)^{-1} \times\left[\ln(1-e^{-B}) - \ln(1-e^{-A})\right] \tag{2}$$

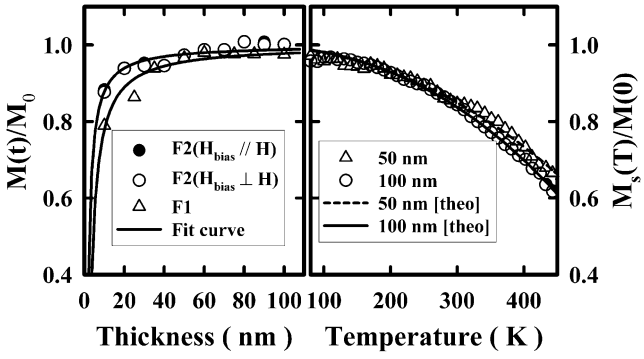


Fig. 8. Reduced magnetization (a) as a function of film thickness for film F1 and F2 and (b) temperature dependence of reduced magnetization for the film F1 with a thickness of 50 and 100 nm. The solid lines denote the theoretical results by using spin-wave theory.

where $M_0$ is the bulk saturation magnetization, $G$, a large number ($\sim 10^7$ or more) which measures the linear dimensions of the film in units of cubic cell, $S$, the spin quantum number of any atom ($S=1/2$), $k$, the Boltzmann constant, $J$, the exchange integral, and

$$A=\frac{16JS}{kT}\left[\left(1+\pi^2/4G^2\right)-\left(1-\pi^2/4G^2\right)\cos k_3\right]$$

$$B=\frac{16JS}{kT}\left[(1+\pi/4)-(1-\pi/4)\cos k_3\right] \quad (3)$$

$$k_3=\frac{2\pi\lambda_3}{G_3}$$

With $G_3=t/a_0$ as $G_i$ is the number of cubic cells in the $i$th direction of crystal, $t$ the film thickness, and $a_0$ is the lattice constant ($a_0=3.592$ Å for $Fe_{64}Ni_{36}$ [11]). The theoretical model given by Eq. (2) was applied to the experimental data. In all cases we have taken $G=1\times10^7$ and considered only $\lambda_3=0$ and 1 to simplify the Eq. (2). From this fit, $M_0$ is 1388 and 1327 emu/cm$^3$ for film F1 and F2, respectively. The values of $M_0$ for F1 and F2 are larger than 1114 emu/cm$^3$ for bulk $Fe_{64}Ni_{36}$ [18]. The parameter $kT/J$ is determined to be 5.34 ($\lambda_3=0$) and 1.79 ($\lambda_3=1$) for film F1, and also 3.75 ($\lambda_3=0$) and 1.44 ($\lambda_3=1$) for film F2.

### 3.5. Temperature dependence of magnetization

Fig. 8b shows the temperature dependence of the magnetization for the film F1 with thickness of 50 and 100 nm. According to the spin-wave theory, the temperature dependence of the magnetization is given by Eq. (4) [19]

$$\frac{M(T)}{M(0)}=1-\beta T^{3/2}-\gamma T^{5/2} \quad (4)$$

where $M(0)$ is the magnetization at 0 K, and $\beta$, $\gamma$ are best-fit constants. The second term is the familiar Bloch $T^{3/2}$ law, while the third one is due to higher order terms in the magnon dispersion relation. From the fitting result of the experimental data within the temperature range of 100–450 K by using Eq. (4), the values of $M(0)$, $\beta$ and $\gamma$ were determined to be 1644 emu/cm$^3$, $2.02\times10^{-5}$ K$^{-3/2}$ and $4.24\times10^{-8}$ K$^{-5/2}$ for the film thickness 50 nm and also 1715 emu/cm$^3$, $1.80\times10^{-5}$ K$^{-3/2}$ and $6.27\times10^{-8}$ K$^{-5/2}$ for the film thickness 100 nm. By conventional linear spin wave theory, $\beta$ is related to the spin wave stiffness constant $D$ through the expressions [19]

$$D=\frac{k}{4\pi}\left(\frac{\varsigma(3/2)g\mu_B}{M(0)\beta}\right)^{2/3} \quad (5)$$

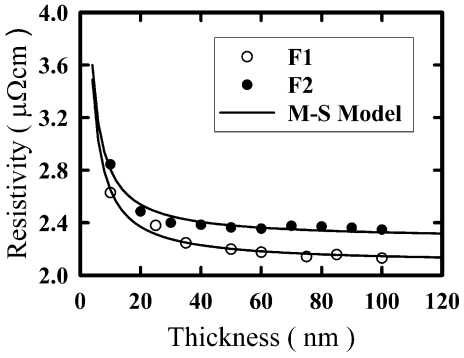


Fig. 9. The resistivity of Fe–Ni films as a function of film thickness for the film F1 and F2. The solid lines are the theoretical values fitted by using Mayadas–Shatzkes model.

where $\varsigma(3/2)=2.612$ is the Riemann zeta function, $g$ the spectroscopic splitting factor, $\mu_B$ the Bohr magnetron and $k$ the Boltzmann constant. The value of $g=2.096$ [20] was used in the present analysis. In evaluating the expression of Eq. (5) for the temperature regime, we found that the values of the spin wave stiffness constant $D$ is 133.03 and 138.73 meV Å$^2$ for the film thickness of 50 and 100 nm, respectively. These values can be compared with $D=132.33$ meV Å$^2$ for the bulk $Fe_{60}Ni_{40}$ [21]. Recently, the temperature dependence of magnetization for a $\gamma$-Ni–Fe alloy in the wide temperature range 85–600 K is analyzed by Eq. (6) using the idea of Kubo and Oguchi [22–24].

$$\frac{M(T)}{M(0)}=1-A\left(\frac{kT}{J}\right)^{3/2}-B\left(\frac{kT}{J}\right)^{5/2} \quad (6)$$

where $A$ and $B$ are best-fit constants and $k$ is the Boltzmann constant. In this case we have taken $A=1.93\times10^{-2}$ and $B=5.25\times10^{-3}$ [24]. The $J$ represents the strength of the interaction between neighboring magnetic ions in the sample and provides a measure of the range of the magnetic interaction. The strength of the interaction $J/k$ for the film thickness 50 and 100 nm from the relation between Eqs. (4) and (6) was determined to be 110.13 and 103.95 K, respectively. Therefore, the value of $J/k$ and $M(0)$ for the films can be compared with 170.99 K of the $Fe_{55}Ni_{45}$ [24] and 1420 emu/cm$^3$ of $Fe_{60}Ni_{40}$ at 4.2 K [25], respectively.

### 3.6. Thickness dependence of electrical resistivity

Fig. 9 shows the thickness dependence of the resistivity of the Fe–Ni films. It is seen that the resistivity decreases with increasing film thickness and the resistivity of film F2 is greater than that of film F1. The resistivity of a polycrystalline metal film has a contribution due to scattering of conduction electrons from phonons and defects (Fuchs–Sondheimer theory) [26]

and from grain boundaries (Mayadas–Shatzkes model) [27]. Several approximations have been derived from the Mayadas–Shatzkes model for the resistivity of a polycrystalline film. The thickness dependence of the resistivity for the films was fitted by using the Eq. (7) under the assumption that the average grain diameter is equal to the thickness [28]

$$\rho = \rho_0 + \left[\frac{3}{2}\left(\frac{R}{1-R}\right) + \frac{3}{8}(1-p)\right]\frac{\rho_0 l_0}{t} \quad (7)$$

where $\rho_0$ is the resistivity of an infinitely thick film, $l_0$ the bulk mean free path, $t$ the thickness of film, $R$ the reflection coefficient, and $p$ the specularity parameter. In the analysis, assuming $p=0$, $l_0$ and $\rho_0$ for film F1 and F2 are found to be 1.3 nm and 2.1 $\mu\Omega$ cm, 1.1 nm and 2.3 $\mu\Omega$ cm, respectively. The reflection coefficient $R$ for the films is found to be approximately 0.5 regardless of deposition condition. The $\rho_0$ estimated from the thickness dependence of the resistivity is smaller than the bulk resistivity (60Fe–40Ni:$\rho_0=60$ $\mu\Omega$ cm [29]).

## 4. Conclusions

In conclusion, we have seen the effect on the physical parameters of Fe–Ni films deposited without and with a constant magnetic bias field. It was shown that the area ratio, $A(1\,1\,1)/A(2\,0\,0)$, of XRD peak for the films without a bias field is nearly constant, but the ratio for the films with the field decreases rapidly with increasing film thickness. The reflection peak of (1 1 1) shows stronger preferred orientation than that of (2 0 0) for the films with a bias field. Magnetic uniaxial anisotropy constant $K_u$ and field $H_k$ of the films with a bias field decrease with increasing film thickness, except for the 40 nm thick film, which has an anomalously large value. The thickness dependence of coercivity for the films without a bias field followed the Bloch wall type. The films with a bias field, however, have a wall type transition from Bloch to Néel at approximately 40 nm. The spin-wave theory was applied to the temperature and thickness dependence of magnetization. The resistivity of the Fe–Ni films was explained by using the Mayadas–Shatzkes model and this model was in good accord with the experimental results.

## Acknowledgments

This work was supported by Korea Research Foundation Grant (KRF-2002-015-CP0113).

## References

[1] C.E. Guillaume, C. R. Acad. Sci. 125 (1897) 235.
[2] J. Crangle, G.C. Hallam, Proc. R. Soc. Lond. A 272 (1963) 119.
[3] E. Hoffmann, H. Herper, P. Entel, S.G. Mishra, P. Mohn, K. Schwarz, Phys. Rev. B 47 (1993) 5589.
[4] G. Dumpich, J. Kästner, U. Kirschbaum, H. Mühlbauer, J. Liang, Th. Lübeck, E.F. Wassermann, Phys. Rev. B 46 (1992) 1058.
[5] D.O. Smith, G.P. Weiss, K.J. Harte, J. Appl. Phys. 37 (1966) 1464.
[6] L. Valenta, Phys. Status Solidi 2 (1962) 112.
[7] M.J. Klein, R.S. Smith, Phys. Rev. 81 (1951) 378.
[8] J. Hubbard, Phys. Rev. B 23 (1981) 5974.
[9] Powder Diffraction file, Joint Committee on Powder Diffraction Standards, ASTM, Philadelphia, PA, 1980, Card 471405.
[10] R.C. O'Handley, Modern Magnetic Materials: Principles and Application, John Wiley & Sons, Inc, New York, NY, 1999, p. 180.
[11] W.B. Pearson, Handbook of Lattice Spacing and Structures of Metals and Alloys, Pergamon Press, London, 1958, p. 640.
[12] E.C. Stoner, E.P. Wolhfarth, Phil. Trans. A 240 (1948) 599.
[13] M. Takahashi, D. Watanabe, T. Kono, S. Ogawa, J. Phys. Soc. Jpn. 15 (1960) 1351.
[14] L. Néel, J. Phys. Rad. 17 (1956) 250.
[15] H.G. Min, S.H. Kim, M. Li, J.B. Wedding, G.C. Wang, Surf. Sci. 400 (1998) 19.
[16] S. Middelhoek, J. Appl. Phys. 34 (1961) 1054.
[17] S.J. Glass, M.J. Kein, Phys. Rev. 109 (1958) 288.
[18] J. Crangle, G.C. Hallam, Proc. Phys. Soc. A 272 (1963) 119.
[19] U. Krey, Z. Phys. B 31 (1978) 247.
[20] A.J. Meyer, G. Asch, J. Appl. Phys. 32 (1961) 330S.
[21] I. Nakai, F. Ono, O. Yamada, J. Phys. Soc. Jpn. 52 (1983) 1791.
[22] R. Kubo, Phys. Rev. 87 (1952) 568.
[23] T. Oguchi, Phys. Rev. 117 (1960) 123.
[24] J.G. Kim, K.H. Han, J.Y. Jenog, J.S. Lee, X.Y. Qin, K.H. Shin, J. Kor. Phys. Soc. 38 (2001) 387.
[25] R.W. Cochrance, G.M. Graham, Can. J. Phys. 48 (1970) 264.
[26] E.H. Sondheimer, Adv. Phys. 1 (1952) 1.
[27] A.F. Mayadas, H. Shatzkes, Phys. Pev. B 1 (1970) 1381.
[28] M.A. Angadi, L.A. Udachan, Thin Solid Films 78 (1981) 299.
[29] R.W. Cahn, P. Haasen, E.J. Kramer, Materials Science and Technology: Volume 3B, Electronic and Magnetic Properties of Metals and Ceramics Part II, VCH Publishers Inc, New York, 1994, p. 439.